Biosensors and Bioelectronics 83 (2016) 267–273

Contents lists available at ScienceDirect

Biosensors and Bioelectronics

journal homepage: www.elsevier.com/locate/bios

A versatile fluorescent biosensor based on target-responsive graphene oxide hydrogel for antibiotic detection

Bing Tan, Huimin Zhao *, Lei Du, Xiaorong Gan, Xie Quan

Key Laboratory of Industrial Ecology and Environmental Engineering (Ministry of Education, China), School of Environmental Science and Technology, Dalian University of Technology, Linggong Road 2, Dalian 116024, PR China

ARTICLE INFO

Article history:
Received 22 February 2016
Received in revised form
12 April 2016
Accepted 20 April 2016
Available online 22 April 2016

Keywords:
GO hydrogel
Aptamer
Fluorescent detection
Antibiotic
Oxytetracycline
Sulfadimethoxine

ABSTRACT

A fluorescent sensing platform based on graphene oxide (GO) hydrogel was developed through a fast and facile gelation, immersion and fluorescence determination process, in which the adenosine and aptamer worked as the co-crosslinkers to connect the GO sheets and then form the three-dimensional (3D) macrostructures. The as-prepared hydrogel showed high mechanical strength and thermal stability. The optimal hydrogel had a linear response for oxytetracycline (OTC) of 25–1000 μg/L and a limit of quantitation (LOQ) of 25 μg/L. Moreover, together with the high affinity of the aptamer for its target, this assay exhibited excellent sensitivity and selectivity. According to its design principle, the as-designed hydrogel was also tested to possess the generic detection function for other molecules by simply replacing its recognition element, which is expected to lay a foundation to realize the assembly of functionalized hierarchical graphene-based materials for practical applications in analytical field.

1. Introduction

Antibiotics, with the ability to kill or inhibit the growth of bacteria, have gained extensively production and application in human and veterinary medicine worldwide during the past decades (Ur Rehman et al., 2015). However, the booming antibiotics consumption in human and animal medicine can directly or indirectly enter into humans, animals, food, and environment (Gao et al., 2015; Wang et al., 2014a; Zhang et al., 2015), which have been emerging contaminants in the environment with much concern for their possible threats to aquatic environment and human health (Liu and Wong, 2013). Moreover, antibiotic use has increased the frequency of resistance genes (Su et al., 2014), which have been an impending threat to public health all over the world. Tetracyclines are a group of broad-spectrum antibiotics, especially OTC has been extensively used as the veterinary antibiotic to prevent bacterial infections in livestock and increase their growth rate because of its effective antimicrobial properties. Unfortunately, the abuses of tetracyclines have caused accumulation of antibiotics in environmental media and food products (An et al., 2015; Ma et al., 2015) and posed serious implications for human health through food chain transmission (Wang et al., 2015). Consequently, it is urgently needed to provide a simple and effective approach to monitor OTC concentration for early warning. Unfortunately, the previously reported methods, including high performance liquid chromatography (HPLC) (Rabolle and Spliid, 2000), enzyme-linked immunosorbent assays (ELISA) (Aga et al., 2003), Surface Enhanced Raman Scattering (SERS) (Li et al., 2013), and amperometric or antibody-based colorimetric methods (Vega et al., 2007; Weber et al., 2005), suffered from tedious sample pretreatment and analysis procedures, possible false positive signals and low specificity of tetracycline derivatives, thus failing to meet the requirements in the fields of environmental monitoring and food safety. Hence, it is imperative to develop rapid, accurate sensing method equipped with specific recognition elements.

In recent years, aptamers application in analytical fields has received extensive concerns (Liu et al., 2009). In essence, aptamers are a class of small, single-stranded RNA or DNA nucleic acids with unique 3D structures that can recognize and bind to their cognate targets with high specificity and affinity, with dissociation constants typically within the pico- to nanomolar range (Nimjee et al., 2005). Generated by systematic evolution of ligands by exponential enrichment (SELEX), aptamers are often referred to as “chemical antibodies” with the unique features of easy modification, high stability, anti-degradation, and so on (Parekh et al., 2010). Moreover, the outstanding specificity of aptamers, far superior to antibodies, makes themselves attractive in small molecule targets detection (Feng et al., 2014). During recent years, aptamers have been optimized and gradually applied in antibiotic sensors design, including detection of tetracycline (Wang et al., 2014b), OTC (Lu et al., 2015), sulfadimethoxine (SDM) (Liu et al.,

* Corresponding author.
E-mail address: zhaohuim@dlut.edu.cn (H. Zhao).

http://dx.doi.org/10.1016/j.bios.2016.04.065
0956-5663/

2014), chloramphenicol (Miao et al., 2016), kanamycin (Guo et al., 2015), and streptomycin (Danesh et al., 2016). Since the aptamer sequences specifically binding to OTC were firstly selected by Niazi et al. (2008), several OTC aptasensors have been reported, including electrochemical, optical and microcantilever methods (Kim et al. 2009, 2010 and Hou et al., 2013). However, these sensors commonly suffered from certain drawbacks, such as unavoidable background colorimetric signal, time-consuming immobilization and washing steps and so on. Therefore, it is still a challenge to develop novel sensing strategy for high-performance determination of antibiotics.

GO hydrogel has been systemically investigated during last several years (Xu et al., 2015), soon after the gelation of GO was first observed during the preparation of large-size GO sheets (Luo et al., 2009). Generally, GO can form a stable aqueous dispersion with a concentration as high as 10 mg/mL (Lin et al., 2011). It is believed that the GO sheets are stabilized in water by edge-bound carboxyl moieties, along with the ample amount of hydrophilic epoxy and hydroxyl groups on their basal planes (Konkena and Vasudevan, 2012). While with the assistance of various promoters, GO sheets can readily self-assemble into hydrogels. Polymers, small ammonium salts, metal ions, aromatic monomer, small biomolecule, as well as sonication and pH and so on were considered to facilitate GO gelation by breaking the electrostatic repulsion balance between the negative charged carboxyl moieties (Li and Shi, 2014). These cross-linkers induce the gelation by different supramolecular interactions, including hydrogen bonding, π-π stacking, static or hydrophobic interactions, and coordination (Bai et al., 2011). Those feasibilities of GO sheets into solid 3D macroscopic hydrogels have been deemed to be conducive to their practical application (Shen et al., 2015), including drug release, water purification, supercapacitors and so on (Li and Shi, 2014). More recently, GO-based macrostructures (hydrogels or aerogels) have also been employed in sensor design. For example, Hoa et al. had designed two glucose sensors based on GO hybrid hydrogel. The hybrids increased both the surface area of 3D networks and the electrocatalytic activity of the redox reactions, which resulted in highly improved glucose sensitivity (Hoa et al., 2016, 2015). Li et al. developed a facile approach to grow Au nanoparticles on highly porous 3D graphene hydrogel with large electroactive surface area and high electrocatalytic activity toward NO oxidation, realizing the in situ detection of NO released from living cells (Li et al., 2015).

Previous sensing applications of 3D macroscopic architectures mainly utilized their electrochemical characteristics. However, the electrochemical measuring techniques require tedious modification of electrodes, which are adverse to their extensive application. Herein, a fluorescent assay based on target-responsive GO-based hydrogel was first time employed for antibiotic detection to the best of our knowledge. The hydrogel can be easily prepared by physically mixing GO sheets, adenosine and aptamers together, avoiding time-consuming immobilization or modification procedures and high temperature and pressure consumption. Moreover, the quantitative detection of OTC was implemented under mild conditions by a facile and fast gelation, soaking, and fluorescence detection process. Based on the design principle, the proposed sensor displayed generic detection function and potential possibility for muti-target detection. Compared with the previously reported methods, the hydrogel sensing platform is believed possessing a certain thermal or chemical stability, which would get a promising application in real environmental samples.

2. Materials and methods

2.1. Materials

The fluorescein amidite (FAM) labeled OTC binding aptamer and SDM aptamer (OTC aptamer: 5′-FAM-CGTACGGAATTCGCTAGCCGAGGCACAGTCGCTGGTGCCTACCTGGTTGCCGTTGTGTGGATCCGAGCTCCACGTG-3′, SDM aptamer: 5′-FAM-GAGGGCAACGAGTGTTTATAGA-3′) were synthesized by Sangon Biotech Co., Ltd. (Shanghai, China) and purified by high-performance liquid chromatography (HPLC). Adenosine, OTC, tetracycline, chlortetracycline, metacycline and doxycycline were purchased from Aladdin Reagent Co., Ltd. (Shanghai, China). SDM was provided by Tokyo Chemical Industry CO., Ltd. Phosphate buffer solution (PBS, 20 mM, pH=7.5) was prepared by mixing the stock solution of Na_2HPO_4 and NaH_2PO_4. All other chemicals were obtained from Sinopharm Chemical Reagent Co., Ltd. (Shanghai, China) and were of analytical grade without additional purification. All solutions were prepared with ultrapure water (Milli-Q water, 18.2 MΩ · cm) from a Millipore Milli-Q system (Bedford, MA, USA).

2.2. Preparation of GO-based hydrogel

The detailed procedures of preparing typical GO-Adenosine hydrogel are available in Supplementary material.

2.3. Antibiotics detection

All the details for detection processes are recorded in Supplementary material.

2.4. Instruments

In this study, several techniques were used to characterize the hydrogels, and the descriptions of the instruments as well as the conditions can be found in Supplementary material.

3. Results and discussion

3.1. GO-based hydrogelation and detection mechanism

GO hydrogels can be readily prepared by physically mixing GO solution with adenosine. The fast gelation of the GO dispersion in the presence of adenosine may attribute to the strong hydrogen bonding and electrostatic interactions between the adenosine and the GO nanosheets. It can be noted that adenosine contain more than one nitrogen (N)-containing functionality (Fig. S1a in Supplementary material). These nitrogen (N)-containing basic functionalities can accept protons from the carboxylic acid groups (–COOH) of the GO sheets (Fig. S1b in Supplementary material) to participate in acid-base-type electrostatic attraction. Furthermore, nitrogen (N)-containing functionalities of adenosine can form hydrogen bonds with hydroxyl groups (–OH), as well as the carboxylic acid groups (–COOH) of GO sheets. For the detection functional hydrogels, aptamers, as a kind of typical functional single-stranded DNA (ssDNA), were added as recognition element. Single-stranded DNA (ssDNA) has been widely applied in noncovalent functionalization or assembly on two dimensional (2D) GO sheets in previous research (Huang et al., 2015; Zhu et al., 2016). In these GO/DNA composite assemblies, ssDNA chains flatly lay on the surfaces of GO sheets as a result of the strong π-π stacking interactions between the hexagonal cells of graphene and the ring structure of nucleobases in ssDNA (Zhu et al., 2015). The π-π stacking interactions between DNA and GO sheets have been elucidated as an effective driving force for assembling GO sheets

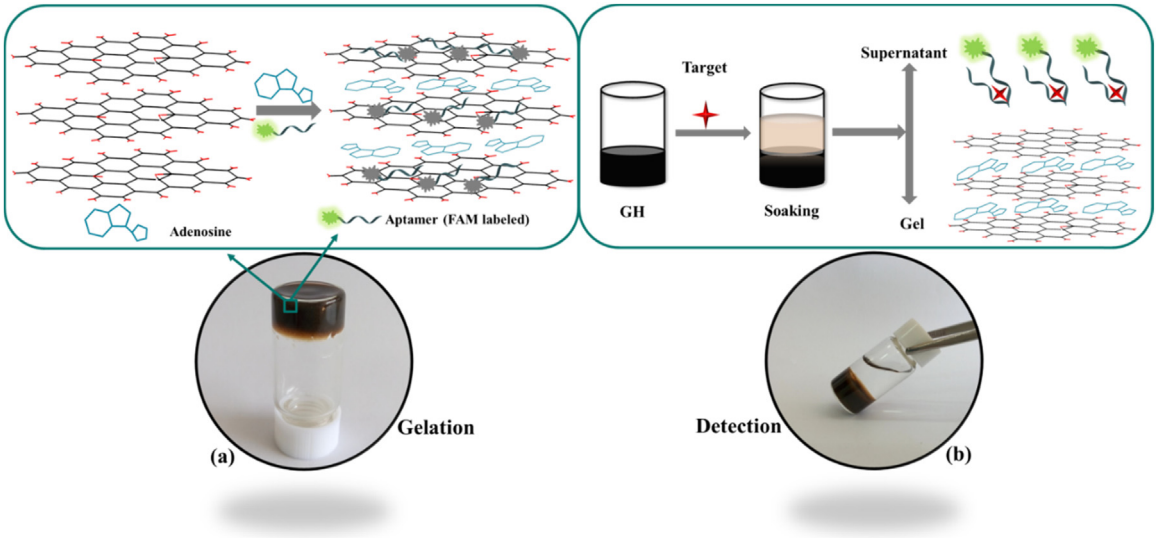

Scheme 1. Schematic of the fabrication of (a) 3D macroscopic hydrogel and (b) the mechanism of selective detection of antibiotic.

into hydrogels (Xu et al., 2010b). Previous studies have employed either nucleosides or DNA as cross-linking agent for fabrication of GO hydrogels with the purpose of exploring gelation mechanism (Adhikari et al., 2012; Xu et al., 2010b). In present research, adenosine and aptamer were served together as cross-linkers between the GO sheets, as illustrated in Scheme 1a. Since aptamer is of a functional ssDNA or RNA with unique 3D structures that can recognize and bind to their cognate targets with high specificity and affinity, these functional hydrogels were prepared primarily aiming at target detection.

Antibiotic aptamers with FAM labeling were applied in our study. The aptamer probe was adsorbed on the GO sheets via the strong π–π stacking interactions and the fluorescence of FAM was quenched by GO sheets due to the fluorescence resonance energy transfer (FRET) (Gao et al., 2014; Huang et al., 2015). When the GO-based functional hydrogel was thoroughly immersed in antibiotic solutions, because of the presence of corresponding antibiotic target, the aptamer would prefer to capture the antibiotic molecule to form a target-aptamer complex. The conformational change will induce a steric hindrance, which would sharply weaken the binding force between FAM labeled aptamer and GO sheets and conduce to the desorption of the complex from GO surface to the supernatant. The increased distance between FAM and GO sheets blocked the FRET process, thus resulting in fluorescence recovery, which facilitated the quantitative detection of antibiotics, as illustrated in Scheme 1b. In contrast, in the absence of antibiotic, the integrated structure of the aptamer probe would remain adsorbed on GO sheets. Additionally, adenosine kept working as the cross-linker to support the macroscopic 3D network structure of the hydrogel during the whole soaking process, avoiding the interference to the fluorescence restoration in the supernatant resulting from hydrogel collapse.

3.2. Characterization of GO-based hydrogel

The as-prepared hydrogel contains about 97% water (by weight), while monomers (GO sheets) and cross-linkers only contribute to 3% of the whole wet weight. The lyophilized GH_0 was employed to investigate on the interior morphology of these hydrogels. Compared with the wrinkled surface of 2D GO sheets (Fig. 1a), the typical SEM image of hydrogel (Fig. 1b) showed a well-defined and interconnected 3D network composed of 2D GO sheets, with pore sizes ranging from submicrometer to several micrometers. The pore walls consisted of thin layers of twisted and curved GO sheets, which were connected by adenosine molecules. It should be noted that the 3D porous structure was in favor of aptamer release from hydrogel (Xu et al., 2010b), which makes it possible to realize the quantitative detection of antibiotics. Furthermore, the structure was characteristic of an enhanced surface area, as well as adsorption capacity, which had been further illustrated by dyes adsorption experiments (Fig. S2 in Supplementary material).

It should be noted that these interior microstructures could ascribe to the hydrogen bonding and acid-base type electrostatic

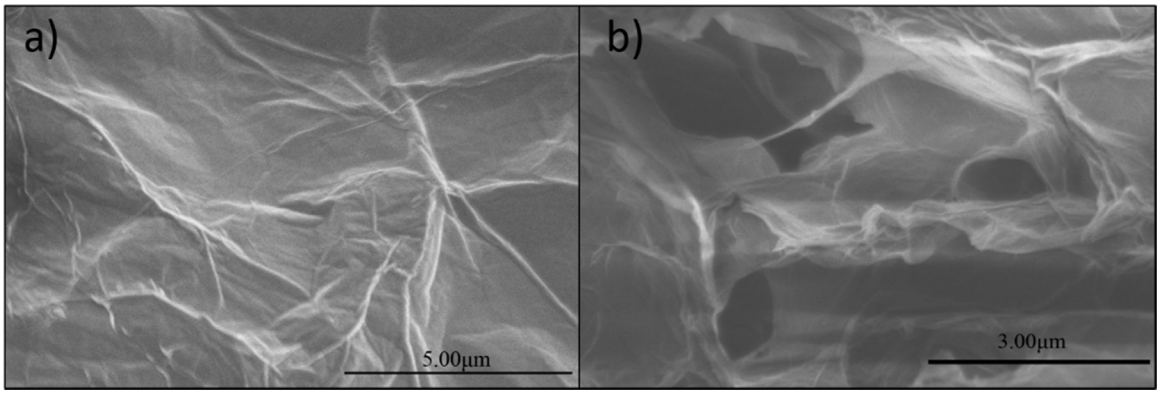

Fig. 1. SEM images of (a) 2D GO sheets and (b) lyophilized GH_0.

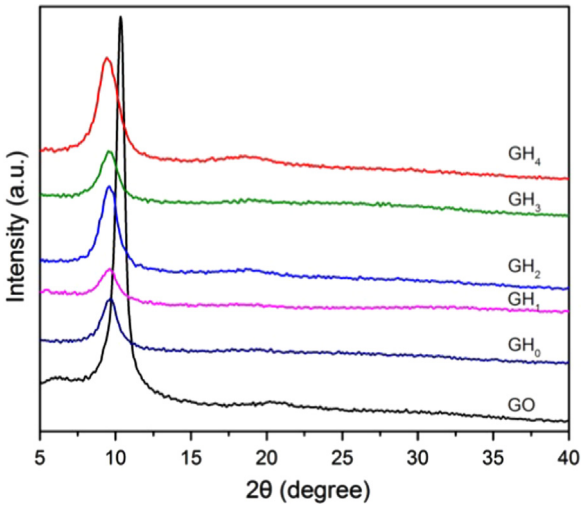

Fig. 2. XRD patterns of freeze-dried GO and GO-based hydrogels.

interactions between adenosine and GO sheets, which validly promote the gelation of original dispersive GO sheets in aqueous solutions. The binding of adenosine to GO sheets was confirmed by Raman spectroscopy. As can be seen in Fig. S3, the typical G band of GO was at 1598 cm^{-1}, with a disordered-induced D band at 1355 cm^{-1}. While in the Raman spectrum of GH_0, the characteristic G and D band of GO sheets were found to be shifted to 1593 cm^{-1} and 1348 cm^{-1}, respectively, indicating a significant strong coupling and charge transfer between the adenosine and GO sheets (Ai et al., 2012).

As for these functional hydrogels with the purpose of antibiotic detection, aptamers were also tested to be favorable for the gelation of GO sheets in aqueous solutions. Fig. 2 illustrates the XRD patterns of the lyophilized GO-based hydrogel with varying concentrations of aptamers and the lyophilized GO. Pure GO showed a characteristic diffraction peak at 10.30°, corresponding to an interlayer distance of 8.58 Å. Compared with pure GO, the 2θ peak of lyophilized GH_0 turned to a smaller angle of 9.70° with an increased layer-to-layer stacking space of 9.11 Å, which further elucidated the strong non-covalent interactions between adenosine and GO sheets (Adhikari et al., 2012). Upon adding aptamers, the XRD peaks of GH_1, GH_2, GH_3 and GH_4 had exhibited a slight downshift in contrast with GH_0. As demonstrated in Fig. 2, along with the increase of aptamer concentrations, the 2θ peaks of GH_1, GH_2, GH_3 and GH_4 could be blue-shifted to 9.63°, 9.58°, 9.55° and 9.43°, corresponding to enhancive inter-planar spacing of 9.17 Å, 9.22 Å, 9.25 Å and 9.37 Å, respectively. It's obvious that aptamers also participate in gelation behaviors of GO sheets. Adenosine and aptamers as mutually reinforced cross-linkers, acted as "glues" for binding GO sheets together to form 3D macrostructures, which are similar to the cases of these cross-linkers induced GO gelation (Ai et al., 2012; Xu et al., 2010b).

Viscoelastic properties of these GO-based hydrogels were examined by rheological tests. It can be mentioned that storage modulus (G′) and loss modulus (G″) respectively denote the ability

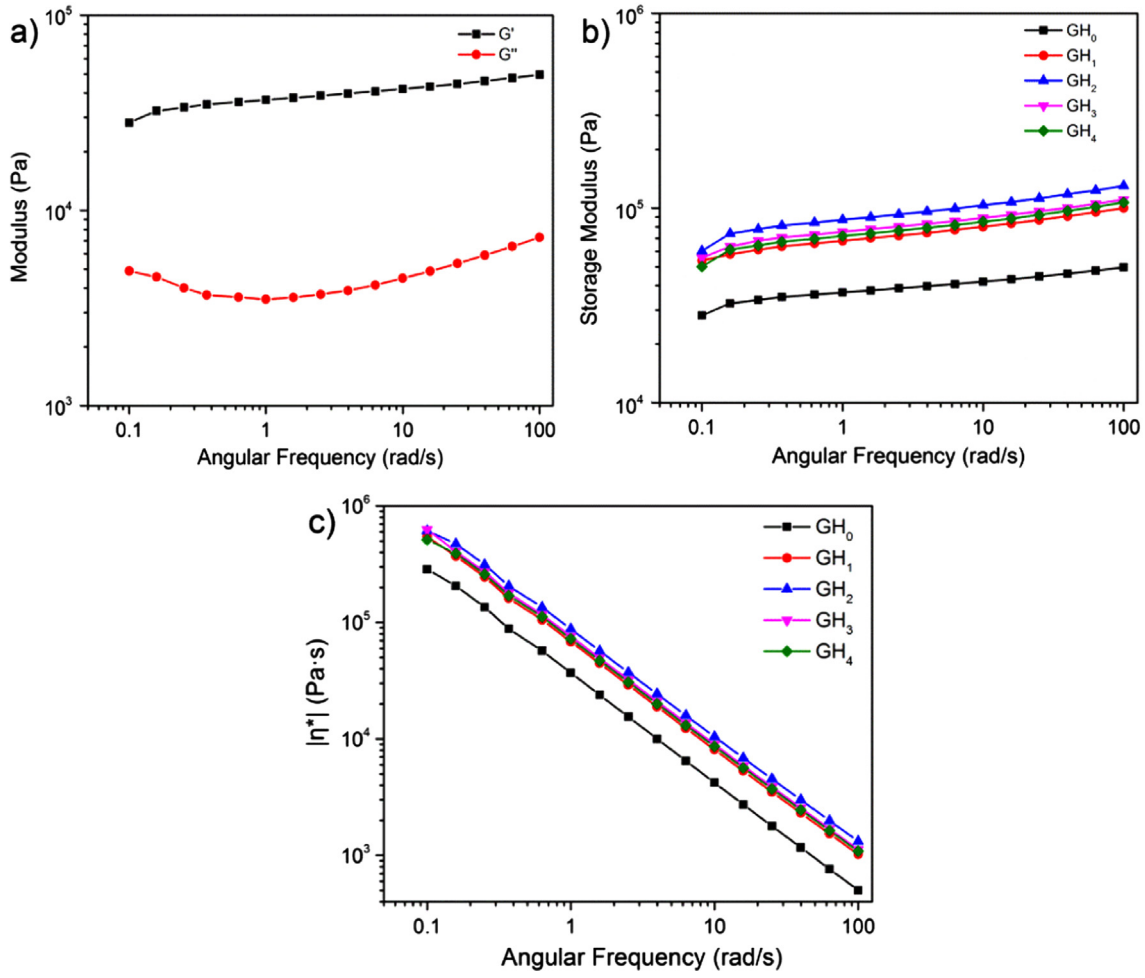

Fig. 3. Dynamic rheology behaviors of GO-based hydrogels. The curves of (a) G′ and G″ of GH_0 *vs* angular frequency; (b and c) G′ and |η*| of GH_0, GH_1, GH_2, GH_3 and GH_4 *vs* angular frequency.

of the deformed material to restore its original geometry and the propensity of a material to flow (Adhikari et al., 2012). As shown in Fig. 3a, the modulus (G′ and G″) of GH_0 exhibited slight frequency dependence over the entire tested frequency range (0.1–100 rad/s). In addition, G′ was about 1 order of magnitude higher than G″ and did not cross over each other during the entire tested range, which implied that elastic response is predominant and the GH_0 had a permanent network with high degree of cross-linking (Xu et al., 2010b). Hydrogels with different contents of aptamers were also studied by dynamic rheological tests (Fig. 3b and c). It was found that both the G′ and dynamic complex viscosity ($|\eta^*|$) of hydrogels entrapped aptamers were higher than GH_0, which was the strong evidence that aptamers also favored gelation and further improved the mechanical strength of the resulting hydrogels. This is mainly on account of the fact that the robustness of the 3D network is enhanced by increasing the cross-linking sites between GO sheets and DNA chains. It was obvious that $|\eta^*|$ values of these GO-based hydrogels had diminished greatly with the increase of the frequency of the applied load, which is the inherent feature of physical cross-linked hydrogels (Xu et al., 2010a). However, we found that the mechanical strength of hydrogels did not present a linear proportionally with the raising of aptamers concentration. Among those hydrogels that anchored different amounts of aptamers, the $|\eta^*|$ values of GH_1, GH_2, GH_3 and GH_4 were approximately equal. Moreover, the G′ of GH_3 and GH_4 were also very close to equal with a slight lower than GH_2 and a little higher than GH_1, which could probably attribute to the fact that excessive addition of aptamers would induce the propensity of the hydrogel to flow and weaken its storage modulus. Although these GO-based hydrogels contained about 97% water, their mechanical properties were still impressive. The G′ of these GO-based hydrogels at 10 rad/s were lower than those hydrothermal or chemical reduced and light irradiated hydrogels (Sui et al., 2011; Wu et al., 2015; Xu et al., 2010a), whereas, they were comparable to most chemically cross-linked GO hydrogels (Adhikari et al., 2012; Huang et al., 2011; Ma et al., 2012; Xu et al., 2010b) and even polymer hydrogels (Banerjee et al., 2009; Sangeetha and Maitra, 2005).

Thermal gravimetric analysis was also employed to discuss the function of aptamers and adenosine in gelation behaviors, and the details are available in Supplementary material.

3.3. Detection of OTC

The quantitative detection of OTC was carried out by measuring the degree of fluorescence restoration. Hydrogel entrapped different amounts of aptamers (GH_1, GH_2, GH_3 and GH_4) were applied to investigate on their detection capability under the optimal reaction time (see Supplementary material). It was believed that there is a certain correlation between the contents of aptamers and the strategy performance. The relationship between the fluorescence intensity and added OTC concentrations were explored in different hydrogel systems. Obviously, there is a common tendency in each hydrogel system that the emission peak at 518 nm gradually increased with increasing the OTC concentration over the range from 0 to 2000 μg/L (Fig. S6 in Supplementary material). This phenomenon was consistent with the design strategy, and was caused by the release of aptamer from the GO sheets to supernatant after the specific combination with target.

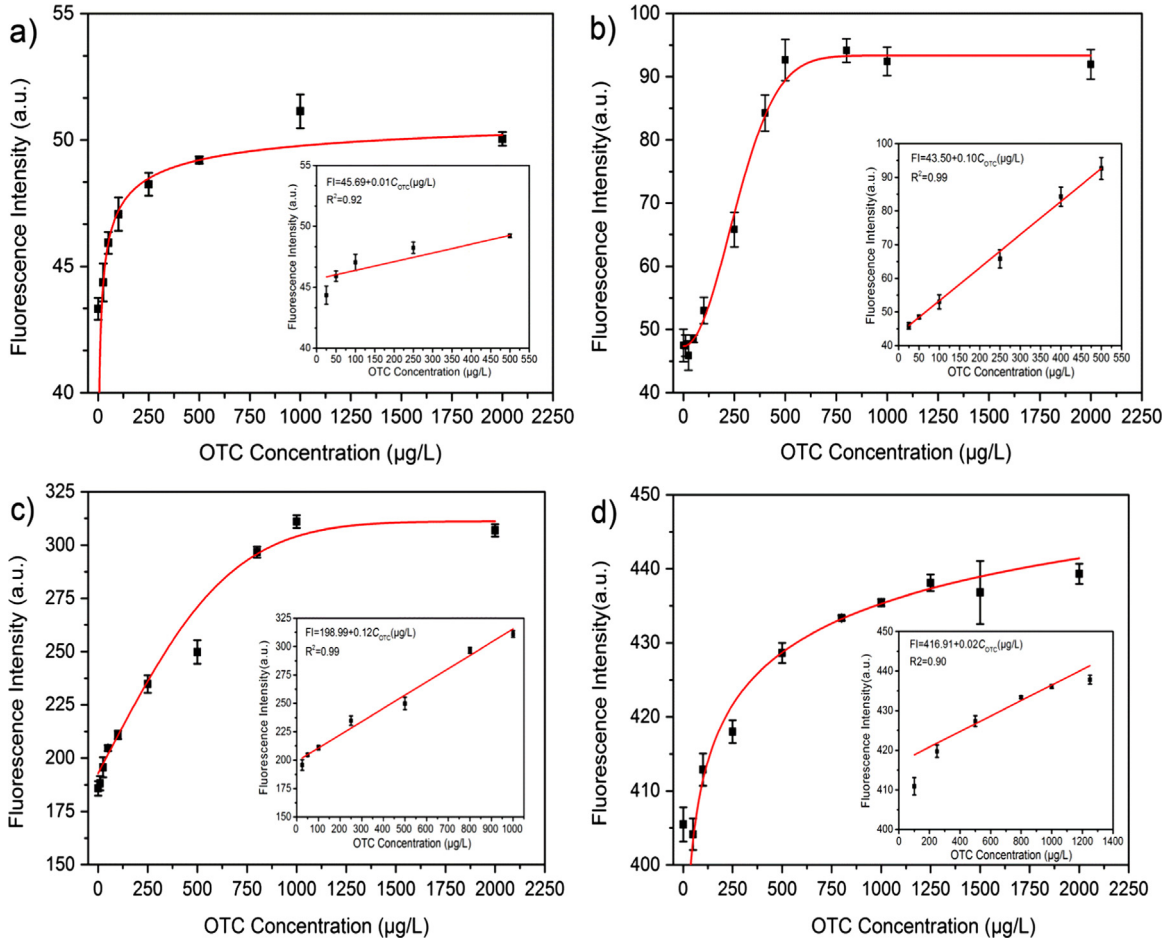

Fig. 4. The plot of fluorescence intensity *vs* OTC concentration in (a) GH_1, (b) GH_2, (c) GH_3, (d) GH_4 hydrogel system. The insets correspond to the linear relationship between the fluorescence intensity and OTC concentration in each hydrogel system.

Table 1
OTC detection in real samples and spiked recoveries.

Sample	Added (μg/L)	Detected (μg/L)	Recovery (%)	RSD (n=3)
Tap water	100	113	113%	1.00%
	250	240	96%	1.75%
Lingshui river	100	117	117%	2.06%
	250	273	109%	2.15%

The associations between the peak intensity and the concentration of OTC were plotted in Fig. 4, which display a typical growth curve model. It was noteworthy that the fluorescence intensity in supernatant climbed up gradually with the increasing of OTC concentration in the beginning, and then did not vary with the OTC concentration after reaching saturation levels. Furthermore, it turned out that the saturation point in each hydrogel system corresponds to different concentrations of OTC. GH_1 and GH_2 showed a relatively fast saturation level at about 500 μg/L, while GH_3 and GH_4 reached saturation levels at about 1000 and 1250 μg/L, respectively, proving that raising the amounts of aptamers would enhance the detection range to some extent.

The linear ranges in different reaction systems, as depicted in the insets to Fig. 4, were obtained. GH_1 and GH_2 shared the same linear relationship ranging from 25 μg/L to 500 μg/L and the regression equation were $FI=45.69+0.01C_{OTC}$ (μg/L) and $FI=43.50+0.10C_{OTC}$ (μg/L), respectively. However, the maximum fluorescence recovery efficiency defined as $(F-F_0)/F_0$ was estimated to be about 13.60% for GH_1 (at 500 μg/L), which was relatively inefficient in contrast with GH_2 (94.48% at 500 μg/L). As for GH_3 and GH_4 that wrapped up more aptamers, they presented a linear response within 25–1000 μg/L and 100–1250 μg/L, and the linear regression equation were $FI=198.99+0.12C_{OTC}$(μg/L) and $FI=416.91+0.02C_{OTC}$(μg/L), respectively. The LOQ was defined as the minimum value tested based on the method, which turned out to be 25 μg/L for GH_1, 25 μg/L for GH_2, 25 μg/L for GH_3 and 100 μg/L for GH_4. In brief, it can be inferred from above that increasing the amounts of recognition elements would effectively improve the upper limitation of this strategy, while in the meantime this could impair the detection sensitivity. Moreover, simply increasing the addition of aptamers would bring about an inevitable excessive background signal, leading to a low fluorescence recovery rate, which had been further confirmed in GH_4 system that the maximum recovery rate was only 8.05%. Conclusively, GH_3 was considered as the best hydrogel in the determination of OTC, since its wider linear and good sensitivity in detection performance, as well as a decent mechanical strength.

Compared with most of recently developed sensor approaches for the detection of OTC (Table S1 in Supplementary material), it was evident that the minimum value of the analytical ranges (LOQs) achieved in the present assay was comparable to the majority of the listed methods and especially superior to those of colorimetric methods, which may be due to the fact that FAM labeling would avoid the color interruptions of background impurities and promote the detection sensitivity. Moreover, there was a wider linear range in comparison with mostly reported fluorescent strategies. The superb linear range was considered to attributed to the fully reaction process in which the prepared hydrogel had been thoroughly immersed in antibiotic solutions for aptamer-target interactions. Accordingly, it could be concluded that the present strategy provided a sensitive and facile approach for the quantitative detection of OTC.

3.4. Specificity and versatility

To evaluate the specificity of this fluorescent assay, the structurally similar tetracycline derivatives had been chosen to investigate on their possible interference with the determination of target OTC under the same experimental procedure. A mixed interference system contained several tetracycline derivatives were also prepared to test its anti-interference ability. As depicted in Fig. S7, the fluorescent emission intensity increased dramatically in response to OTC at 800 μg/L. In contrast, no obvious responses were observed for other tetracyclines at the same concentration. What's more, the developed sensor exhibited a similar response in the mixed tetracyclines solution compared with that in the pure OTC solution, which further demonstrated its superior specificity and anti-interference ability.

According to its design principle, the as-designed hydrogel was of the versatility for other molecules detection (see Supplementary material).

3.5. Detection of OTC in real water samples

The as-prepared optimal hydrogel (GH_3) for OTC detection was applied in real sample analysis to evaluate its feasibility in an actual aquatic environment. Tap water and Lingshui River (Dalian, China) samples were chosen. The pretreatment process can be found in Supplementary material. The spike-and-recovery method was used in this study. As shown in Table 1, the recoveries were acceptable and calculated to be in the range of 96–117% based on the addition of 100 μg/L and 250 μg/L OTC, which indicated that the developed assay could be preliminarily applied for the determination of OTC in real samples. The relative standard deviations (RSDs) also validated the good reproducibility of this strategy.

4. Conclusion

In summary, we have demonstrated the general design for a fluorescent detection platform on the basis of GO-based hydrogel. The as-prepared fluorescent assay for OTC detection showed high sensitivity and selectivity. The linear range was found to be 25–1000 μg/L with a LOQ of 25 μg/L. The developed strategy was also tested to possess the feasibility of *in situ* OTC detection in real samples. Even though the as-fabricated hydrogel is one-off, it is undeniable that this assay is highly sensitive and selective for the environmental monitoring of antibiotic. As no special features on the aptamers are required, our technique might be a generic approach that can be applied with different aptamer sequences for the detection of other molecules. This work provides a new insight for the assembly of functionalized hierarchical graphene-based materials, which will help rational design and fabrication of 3D macroscopic architecture for practical applications, such as water purification, gas adsorption and optical or electrochemical sensors design.

Acknowledgements

This study was supported by the National Natural Science Foundation of China (No. 21277016), the Fundamental Research Funds for the Central Universities (DUT15TD12) and the Program for Changjiang Scholars and Innovative Research Team in University (IRT_13R05).

Appendix A. Supplementary material

Supplementary data associated with this article can be found in the online version at http://dx.doi.org/10.1016/j.bios.2016.04.065.

References

Adhikari, B., Biswas, A., Banerjee, A., 2012. Langmuir 28, 1460–1469.
Aga, D.S., Goldfish, R., Kulshrestha, P., 2003. Analyst 128, 658–662.
Ai, W., Du, Z.Z., Liu, J.Q., Zhao, F., Yi, M.D., Xie, L.H., Shi, N.E., Ma, Y.W., Qian, Y., Fan, Q.L., Yu, T., Huang, W., 2012. RSC Adv. 2, 12204–12209.
An, J., Chen, H., Wei, S., Gu, J., 2015. Environ. Earth Sci. 74, 5077–5086.
Bai, H., Li, C., Wang, X., Shi, G., 2011. J. Phys. Chem. C 115, 5545–5551.
Banerjee, S., Das, R.K., Maitra, U., 2009. J. Mater. Chem. 19, 6649–6687.
Danesh, N.M., Ramezani, M., Emrani, A.S., Abnous, K., Taghdisi, S.M., 2016. Biosens. Bioelectron. 75, 123–128.
Feng, C., Dai, S., Wang, L., 2014. Biosens. Bioelectron. 59, 64–74.
Gao, L., Lian, C., Zhou, Y., Yan, L., Li, Q., Zhang, C., Chen, L., Chen, K., 2014. Biosens. Bioelectron. 60, 22–29.
Gao, M., Qi, Y., Song, W., Zhou, Q., 2015. Chemosphere 139, 229–234.
Guo, W., Sun, N., Qin, X., Pei, M., Wang, L., 2015. Biosens. Bioelectron. 74, 691–697.
Hoa, L.T., Sun, K.G., Hur, S.H., 2015. Sens. Actuator B – Chem. 210, 618–623.
Hoa, L.T., Chung, J.S., Hur, S.H., 2016. Sens. Actuator B – Chem. 223, 76–82.
Hou, H., Bai, X., Xing, C., Gu, N., Zhang, B., Tang, J., 2013. Anal. Chem. 85, 2010–2014.
Huang, C., Bai, H., Li, C., Shi, G., 2011. Chem. Commun. 47, 4962–4964.
Huang, Y., Yang, H.Y., Ai, Y., 2015. Anal. Chem. 87, 9132–9136.
Kim, Y.S., Niazi, J.H., Gu, M.B., 2009. Anal. Chim. Acta 634, 250–254.
Kim, Y.S., Kim, J.H., Kim, I.A., Lee, S.J., Jurng, J., Gu, M.B., 2010. Biosens. Bioelectron. 26, 1644–1649.
Konkena, B., Vasudevan, S., 2012. J. Phys. Chem. Lett. 3, 867–872.
Li, C., Shi, G.Q., 2014. Adv. Mater. 26, 3992–4012.
Li, J., Xie, J., Gao, L., Li, C.M., 2015. ACS Appl. Mater. Interfaces 7, 2726–2734.
Li, Y.T., Qu, L.L., Li, D.W., Song, Q.X., Fathi, F., Long, Y.T., 2013. Biosens. Bioelectron. 43, 94–100.
Lin, Y., Ehlert, G.J., Bukowsky, C., Sodano, H.A., 2011. ACS Appl. Mater. Interfaces 3, 2200–2203.
Liu, J., Cao, Z., Lu, Y., 2009. Chem. Rev. 109, 1948–1998.
Liu, J., Guan, Z., Lv, Z., Jiang, X., Yang, S., Chen, A., 2014. Biosens. Bioelectron. 52, 265–270.
Liu, J.L., Wong, M.H., 2013. Environ. Int. 59, 208–224.
Lu, C., Tang, Z., Liu, C., Kang, L., Sun, F., 2015. Anal. Bioanal. Chem. 407, 4155–4163.
Luo, Z., Lu, Y., Somers, L.A., Johnson, A.T.C., 2009. J. Am. Chem. Soc. 131, 898–899.
Ma, D., Lin, J., Chen, Y., Xue, W., Zhang, L.M., 2012. Carbon 50, 3001–3007.
Ma, Y., Li, M., Wu, M., Li, Z., Liu, X., 2015. Sci. Total Environ. 518, 498–506.
Miao, Y., Gan, N., Li, T., Cao, Y., Hu, F., Chen, Y., 2016. Sens. Actuator B – Chem. 222, 1066–1072.
Niazi, J.H., Lee, S.J., Kim, Y.S., Gu, M.B., 2008. Bioorg. Med. Chem. 16, 1254–1261.
Nimjee, S.M., Rusconi, C.P., Sullenger, B.A., 2005. Annu. Rev. Med., 555–583.
Parekh, P., Tang, Z., Turner, P.C., Moyer, R.W., Tan, W., 2010. Anal. Chem. 82, 8642–8649.
Rabolle, M., Spliid, N.H., 2000. Chemosphere 40, 715–722.
Sangeetha, N.M., Maitra, U., 2005. Chem. Soc. Rev. 34, 821–836.
Shen, Y., Fang, Q., Chen, B., 2015. Environ. Sci. Technol. 49, 67–84.
Su, J.Q., Wei, B., Xu, C.Y., Qiao, M., Zhu, Y.G., 2014. Environ. Int. 65, 9–15.
Sui, Z., Zhang, X., Lei, Y., Luo, Y., 2011. Carbon 49, 4314–4321.
Ur Rehman, M.S., Rashid, N., Ashfaq, M., Saif, A., Ahmad, N., Han, J.I., 2015. Chemosphere 138, 1045–1055.
Vega, D., Agui, L., Gonzalez-Cortes, A., Yanez-Sedeno, P., Pingarron, J.M., 2007. Anal. Bioanal. Chem. 389, 951–958.
Wang, F.H., Qiao, M., Su, J.Q., Chen, Z., Zhou, X., Zhu, Y.G., 2014a. Environ. Sci. Technol. 48, 9079–9085.
Wang, H., Wang, B., Zhao, Q., Zhao, Y., Fu, C., Feng, X., Wang, N., Su, M., Tang, C., Jiang, F., Zhou, Y., Chen, Y., Jiang, Q., 2015. Environ. Sci. Technol. 49, 5070–5079.
Wang, S., Yong, W., Liu, J., Zhang, L., Chen, Q., Dong, Y., 2014b. Biosens. Bioelectron. 57, 192–198.
Weber, C.C., Link, N., Fux, C., Zisch, A.H., Weber, W., Fussenegger, M., 2005. Biotechnol. Bioeng. 89, 9–17.
Wu, J., Chen, A., Qin, M., Huang, R., Zhang, G., Xue, B., Wei, J., Li, Y., Cao, Y., Wang, W., 2015. Nanoscale 7, 1655–1660.
Xu, Y., Shi, G., Duan, X., 2015. Acc. Chem. Res. 48, 1666–1675.
Xu, Y., Sheng, K., Li, C., Shi, G., 2010a. ACS Nano 4, 4324–4330.
Xu, Y., Wu, Q., Sun, Y., Bai, H., Shi, G., 2010b. ACS Nano 4, 7358–7362.
Zhang, Q.Q., Ying, G.G., Pan, C.G., Liu, Y.S., Zhao, J.L., 2015. Environ. Sci. Technol. 49, 6772–6782.
Zhu, D., Wang, L., Xu, X., Jiang, W., 2016. Biosens. Bioelectron. 75, 155–160.
Zhu, Y.Y., Cai, Y.L., Xu, L.G., Zheng, L.X., Wang, L.M., Qi, B., Xu, C.L., 2015. ACS Appl. Mater. Interfaces 7, 7492–7496.